

Classification and Uncertainty Quantification of Corrupted Data using Semi-Supervised Autoencoders

Philipp Joppich*

AUDI AG, Technical University of Munich
philipp.joppich@audi, tum].de

Sebastian Dorn*

AUDI AG
sebastian.dorn@audi.de

Oliver De Candido, Wolfgang Utschick

Technical University of Munich
[oliver.de-candido, utschick]@tum.de

Jakob Knollmüller

Technical University of Munich
jakob.knollmuller@tum.de

Abstract

Parametric and non-parametric classifiers often have to deal with real-world data, where corruptions like noise, occlusions, and blur are unavoidable — posing significant challenges. We present a probabilistic approach to classify strongly corrupted data and quantify uncertainty, despite the model only having been trained with uncorrupted data. A semi-supervised autoencoder trained on uncorrupted data is the underlying architecture. We use the decoding part as a generative model for realistic data and extend it by convolutions, masking, and additive Gaussian noise to describe imperfections. This constitutes a statistical inference task in terms of the optimal latent space activations of the underlying uncorrupted datum. We solve this problem approximately with Metric Gaussian Variational Inference (MGVI). The supervision of the autoencoder’s latent space allows us to classify corrupted data directly under uncertainty with the statistically inferred latent space activations. Furthermore, we demonstrate that the model uncertainty strongly depends on whether the classification is correct or wrong, setting a basis for a statistical "lie detector" of the classification. Independent of that, we show that the generative model can optimally restore the uncorrupted datum by decoding the inferred latent space activations.

1 Introduction and Motivation

Many real-world applications of data-driven classifiers, e.g., neural networks, involve corruptions that pose significant challenges to the pretrained classifiers. Often, the corruption must previously be included, and thus already be known, during the process of training. For instance, noise (e.g., due to sensor imperfections) and convolutions (e.g., due to lens flares or unfocused images) are inevitable in image processing systems and may occur spontaneously and irregularly. The same holds for masking, which may occur when a foreign object occludes the actual object of interest (e.g., water droplets or dirt or scratches on the camera lens).

Hence, we aim to answer the following question in this paper: How can we classify corrupted data with a parametric classifier trained exclusively on uncorrupted data? As classifying corrupted data naturally demands a measure of uncertainty for validation (corruption may, in the worst case, lead to a total loss of information), we include both model uncertainty δ_m and reconstruction uncertainty δ_r in the classification. We refer to δ_m as the model’s confidence on the classification itself. In contrast,

*Corresponding Authors.

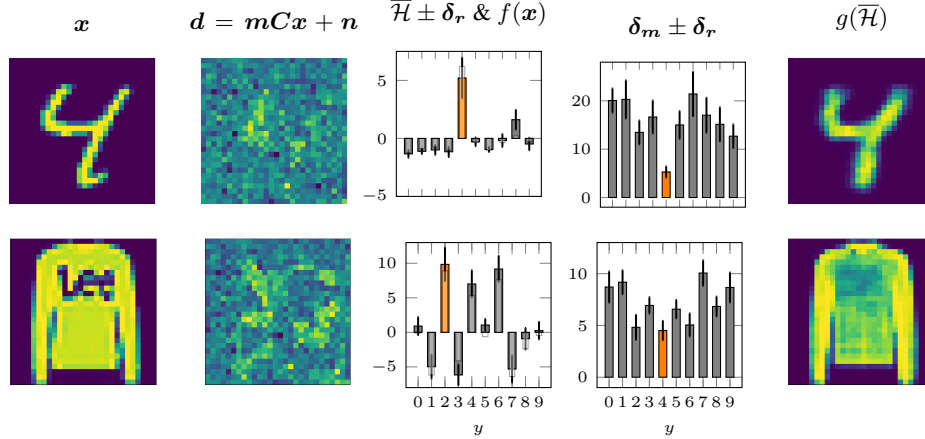


Figure 1: From left to right: Ground truth image x in the data space, corrupted image d in the data space (random masking m , Gaussian blur C , additive white Gaussian noise n), posterior mean $\bar{\mathcal{H}}$ in the latent space with reconstruction uncertainty δ_r , model uncertainty δ_m and the restored image $g(\bar{\mathcal{H}})$ (decoded posterior mean) in the data space. We have included the encoding of the uncorrupted data $f(x)$ (illustrated by the shaded white bars in the third column). Top row: data sample from the MNIST-dataset (ground truth label: 4). Bottom row: data sample from the Fashion-MNIST-dataset (ground truth label: 2 (pullover)). We can classify d using the posterior mean $\bar{\mathcal{H}}$ as the autoencoder’s latent space is supervised (note the highlighted max. activation responsible for classification). We are able to classify and quantify model uncertainty δ_m with the Mahalanobis-distance in the latent space (note the highlighted min. activation responsible for classification). Strong overlapping for the Fashion-MNIST-example of the $1 \cdot \sigma$ error bars of δ_r across different classes indicates that no reliable and confident classification is possible due to heavy corruption.

we refer to δ_r as the confidence of the process on reconstructing the latent space activations given some corrupted datum. An overview of the proposed method is illustrated in Figure 1.

2 Classification and Uncertainty Quantification of Corrupted Data

2.1 Methodology Overview and Related Work

To address the challenge of classification and uncertainty quantification of corrupted data, we propose the following core approach, illustrated in Figure 2.

- ① **In the first step**, we train a semi-supervised autoencoder [1] that is: (a) capable of classifying the input data with its latent space activations \mathbf{h} , and (b) capable of decoding the (supervised) latent space activations to generate higher-dimensional data, targeting it to be identical to the input. Except for these two constraints (a) and (b), we do not impose any further restrictions on the autoencoder and train it as a standard feedforward neural network.
- ② **In the second step**, we decouple the decoder g from the autoencoder and treat the decoder as a fixed generative function g . Neither retraining nor further modifying of g is done in the following steps.
- ③ **In the third step**, we include g in an ADDITIVE WHITE GAUSSIAN NOISE (AWGN) channel-model $d = mCg(\mathbf{h}) + n$. This AWGN channel model additionally involves heavy corruption like convolution C and masking m .
- ④ **In the final step**, we approximate the posterior probability distribution $\mathcal{P}(\mathbf{h}|d)$ in the latent space, and derive the mean and standard deviation, corresponding optimally to some uncorrupted datum $g(\mathbf{h})$, given the corrupted datum d . Due to supervision at the latent space, this reconstruction enables a direct classification of d including model and reconstruction uncertainty quantification, even though the decoding function was trained on uncorrupted data.

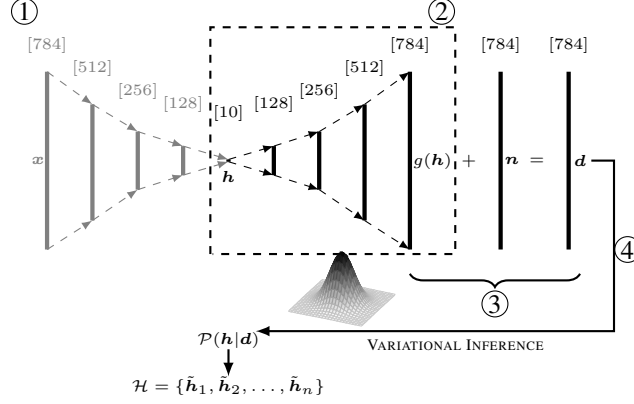


Figure 2: Concept visualization: Steps involved in classifying corrupted data and quantifying uncertainty of the reconstruction, as described in Section 2.1. The arrow from d to $\mathcal{P}(h|d)$ graphically illustrates the process of statistically inferring the latent space activations from corrupted data d using MGVI. \mathcal{H} includes all samples drawn from the posterior distribution in the latent space. Subsequently, the sampling mean and sampling standard deviation are determined from \mathcal{H} to classify corrupted data samples and quantify their reconstruction uncertainty. Model uncertainty is determined via the Mahalanobis distance in the latent space. We do not depict convolution C and masking m in the figure above for simplicity.

We use a set of samples \mathcal{H} from the approximate posterior probability distribution to determine the sampling mean $\text{mean}(\mathcal{H}) = \bar{h}$ as well as the set’s reconstruction uncertainty δ_r with the sampling standard deviation $\text{std}(\mathcal{H})$. Samples are statistically inferred by METRIC GAUSSIAN VARIATIONAL INFERENCE (MGVI) [2].

In addition to reconstruction uncertainty δ_r , we determine the model uncertainty by calculating the MAHALANOBIS-distance (M-distance) [3] in the latent space representation, slightly different to [4]. For details of our implementation, see Algorithm 2 in the appendix. We here distinguish between reconstruction uncertainty δ_r and model uncertainty δ_m to evaluate the confidence of the process of inferring h and to evaluate the confidence of the classification given by the supervised latent space, respectively.

Similarly to our approach, [5], [6] have shown that the reconstruction of the latent space by posterior inference and by using generative models ([7], [8], [9]) for a corrupted datum can lead to an optimal image restoration with uncertainty quantification. These methods do, however, not focus on classifying the corrupted datum in the latent space, nor using supervised autoencoder structures.

In the field of quantifying uncertainties of classifications there exist several methods. Predominantly BAYESIAN NEURAL NETWORKS (BNNs) including neural network ensembling ([10], [11], [12]) and MONTE CARLO-dropout (MC-dropout) [13] have lately shown success. The latter will be compared with our method in Section 3.

Finally, various methods to perform image restoration exist in the literature (see [14], [15], [16], [17], [18]). Similar to the well-known denoising autoencoder [19], almost all methods require prior knowledge of the corruption to be included in the training data. We argue that these methods lack flexibility, as they deal with one specific type of corruption. Once the model is trained, one cannot include other corruption types without retraining.

Moreover, many methods focus on either classification or eliminating corruption, but none of the named approaches combine both.

2.2 Generative Model and Bayesian Inference with Neural Networks

The first step of our method is to train a semi-supervised autoencoder. The autoencoder involves the encoding function f (mapping data $x \in \mathbb{R}^p$ to the latent space representation with activations $h \in \mathbb{R}^z, z \in \mathbb{N}$) as well as the decoding function g (mapping h to the data space representation

$\hat{x} \in \mathbb{R}^p, p \in \mathbb{N}, p \gg z$). Parameters of $f : \mathbb{R}^p \rightarrow \mathbb{R}^z$ and $g : \mathbb{R}^z \rightarrow \mathbb{R}^p$ are optimized via a combination of two loss terms \mathcal{L}_{gf} (representing reconstruction loss in the data space) and \mathcal{L}_f (representing classification loss in the latent space):

$$\mathcal{L}_{\text{SAE}} = \mathcal{L}_{gf}(g(f(x)), x) + \mathcal{L}_f(f(x)^j, y) = \mathcal{L}_{gf}(\hat{x}, x) + \mathcal{L}_f(h^j, y). \quad (1)$$

where j denotes the number of dimensions of \mathbf{h} that are supervised, i.e., $\mathbf{h}^j = [h_1, \dots, h_j]$. The number of classes to be classified equals j . After normalizing all data samples (i.e., pixel values range in between $[0, 1]$), we use the corresponding cross-entropy for each respective loss term to penalize false classifications in the latent space and inaccurate reconstructions in the data space. The binary cross-entropy represents the reconstruction loss, while we use the sparse categorical cross-entropy on integer labels $\mathbf{y} = [0, 1, \dots, 9]$ to represent the classification loss. Note that for training, we process the latent space activations \mathbf{h} through the softmax-function before feeding them to the sparse categorical cross-entropy. However, the softmax-function is not included as an activation function in our neural network. We minimize the general loss function Equation (1) using Adam optimizer [20]².

Once the training procedure has converged, we decouple the decoding function g from the autoencoder and extend it to model different types of corruption (this is necessary as the decoder is trained on uncorrupted data). Without loss of generality, we use an AWGN model including the nonlinearity $g(\mathbf{h})$, which additionally involves masking \mathbf{m} and convolution \mathbf{C} on g :

$$\mathbf{d} = \mathbf{m}\mathbf{C}g(\mathbf{h}) + \mathbf{n}. \quad (2)$$

In the data space, additive white Gaussian noise, $\mathbf{n} \in \mathbb{R}^p \sim \mathcal{N}(\mathbf{0}, \Sigma_n)$, is applied to the decoded latent space signal $g(\mathbf{h})$, which yields the corrupted data $\mathbf{d} \in \mathbb{R}^p$. Note for the implementation of $\mathbf{h} = \mathbf{A}\xi + \mu_h$, the reparametrization trick [21] is applied.³

In addition to AWGN, we include corruptions of masking \mathbf{m} and convolutions \mathbf{C} , which are both linear operations. See the Appendix A, for details on the implementation of \mathbf{n} , \mathbf{m} and \mathbf{C} .

Since we are interested in reconstructing the latent space activation \mathbf{h} from \mathbf{d} alongside uncertainty quantification, the goal is to determine the posterior distribution $\mathcal{P}(\mathbf{h}|\mathbf{d}) \propto \mathcal{P}(\mathbf{d}|\mathbf{h})\mathcal{P}(\mathbf{h})$. The log-probability distribution reads

$$-\ln \mathcal{P}(\mathbf{h}|\mathbf{d}) = \frac{1}{2} \left((\mathbf{d} - \mathbf{m}\mathbf{C}g(\mathbf{h}))^T \Sigma_n^{-1} (\mathbf{d} - \mathbf{m}\mathbf{C}g(\mathbf{h})) + (\mathbf{h}^T \Sigma_h^{-1} \mathbf{h}) \right) + \text{const.}, \quad (3)$$

where $(\cdot)^T$ denotes the matrix transpose. Since we are finally interested in the analytically intractable mean of \mathbf{h} , $\langle \mathbf{h} \rangle_{\mathcal{P}(\mathbf{h}|\mathbf{d})} = \int \mathbf{h} \mathcal{P}(\mathbf{h}|\mathbf{d}) d\mathbf{h}$, we approximately determine mean and variance of $\mathcal{P}(\mathbf{h}|\mathbf{d})$ by applying MGVI. Similar to other variational inference methods ([21], [22]), MGVI approximates the distribution by a simpler, but tractable distribution from within a variational family, $\mathcal{Q}(\mathbf{h})$. The parameters of $\mathcal{Q}(\mathbf{h})$, i.e., mean η and covariance Δ , are obtained by the minimization of the variational lower bound. The size of a full variational covariance scales quadratically with the number of latent variables. Taking these limitations into account, we employ MGVI, which locally approximates the target distribution using the inverse Fisher metric as an uncertainty estimate around the variational mean η , for which we optimize. The approximation is represented by an ensemble of samples $\mathcal{H} = \{\tilde{\mathbf{h}}_1, \tilde{\mathbf{h}}_2, \dots, \tilde{\mathbf{h}}_n\}$ with $\tilde{\mathbf{h}}_n \in \mathbb{R}^z$, which we use for our analysis. $(\tilde{\cdot})$ refers to the inferred sample. We here call $\overline{\mathcal{H}}$ the posterior mean and δ_r the posterior standard deviation, or, the reconstruction uncertainty.

2.3 Classification and Uncertainty Quantification

The supervision of the latent space allows us to classify the input \mathbf{d} in a straightforward manner by evaluating the sampling mean and sampling standard deviation of the set \mathcal{H} . While the sampling mean of the set $\text{mean}(\mathcal{H}) = \overline{\mathcal{H}}$ gives the class of the most likely classification, the sampling standard deviation reflects the reconstruction uncertainty δ_r of the latent space posterior distribution. δ_r depends on the type and magnitude of the corruption as well as the prior probability distribution we include in the channel model (Equation (3)). We visualize this dependency with various experiments, see Figure 4 and Figure 10.

²Test accuracy of [98, 6%; 89, 4%] on the encoding function f with [MNIST; Fashion-MNIST].

³ $\Sigma_h = \text{cov}(f(\mathbf{X}_{\text{val}})), \Sigma_h = \mathbf{A}\mathbf{A}^T, \Sigma_h \in \mathbb{R}^{z \times z}, \xi \sim \mathcal{N}(\mathbf{0}, \mathbf{I}), \xi \in \mathbb{R}^z, \mu_h = \text{mean}(\mathbf{X}_{\text{val}}), \mu_h \in \mathbb{R}^z$

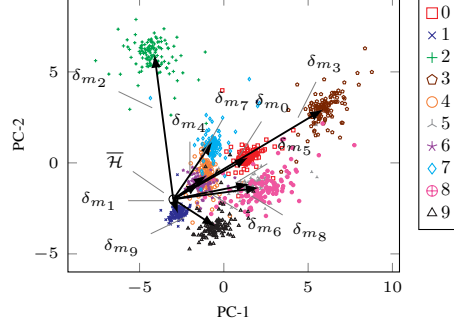


Figure 3: Illustration of the latent space structure of a semi-supervised autoencoder and the M-distance as a classifier based on MNIST. For this visualization, the 10-dimensional latent space activations are mapped to a two-dimensional subspace using a Principal Component (PC) analysis [23]. For an arbitrary corrupted datum \mathbf{d} , the inferred posterior mean $\bar{\mathbf{H}}$ in the latent space is marked accordingly. To classify $\bar{\mathbf{H}}$, the M-distance is computed to every cluster in the latent space to obtain δ_{m_i} for all ten classes. The shortest distance $\arg \min(\delta_m)$ serves as the classification. In this concrete example, the given posterior mean $\bar{\mathbf{H}}$ would likely be classified to digit 1. The absolute value of δ_m reflects at the same time the model uncertainty w.r.t. each class in the latent space.

The straightforward classification does not yet provide information about the model uncertainty on the classification. Since we are additionally interested in the uncertainty of the model, δ_m , we evaluate the M-distance of all samples in \mathcal{H} to all class conditional distributions in the latent space. The closest class conditional distribution to a single sample \mathbf{h}_n corresponds to the most likely class. The absolute value of the M-distance to the closest class conditional distribution serves as a measure of the model uncertainty δ_m . In this work, all class conditional distributions in the latent space are assumed to follow multivariate Gaussian distributions with covariance Σ_i and mean μ_i . We determine the parameters of these class conditional distributions by passing the uncorrupted data samples from an independent (i.e., independent of training and testing) dataset \mathbf{X}_{val} (see Section 3) through the encoder f . This method is an implementation slightly different to [4], where it was shown that the Mahalanobis metric is not only an accurate classifier in this context but also a reliable out-of-distribution detector reflecting the model uncertainty. [4] uses tied covariance matrices instead of individual covariance matrices for each class conditional distribution, as done in our method.

Concretely, we calculate the M-distance of all samples in \mathcal{H} to all class-conditional clusters \mathcal{C}_k within the latent space, each characterized by $\mu_{\mathcal{C}_k}$ and $\Sigma_{\mathcal{C}_k}$ for K -classes. We then determine sampling mean $\bar{\delta}_m$ and sampling standard deviation $\bar{\delta}_r$ of the M-distances of all samples. This way, we can represent reconstruction uncertainty by the sampling standard deviation (resulting directly from the shape of the inferred posterior distribution) and model uncertainty by the absolute value of the M-distance. For a graphical illustration, refer to Figure 3. The pseudo-code is given in Algorithm 2 in the appendix.

2.4 Summary and Limitations

We summarize our proposed methodology (Algorithm 1) to classify a corrupted datum \mathbf{d} including uncertainty quantification, which requires the following input in addition to \mathbf{d} :

\mathbf{m}, \mathbf{C} : Without loss of generality, here we assume corruption by masking and convolution represented by \mathbf{m} and \mathbf{C} in the AWGN channel-model, as written in Equation (2). The convolution \mathbf{C} can be determined with methods proposed by, e.g., [24], [25], [26], occlusion \mathbf{m} can be modeled by, e.g., [27], [28].

Σ_n : Noise covariance matrix. Noise is drawn from a Gaussian distribution with covariance Σ_n and mean $\mu_n = \mathbf{0}$ and applied additively to the data \mathbf{d} . Various methods exist to extract Σ_n given \mathbf{d} (e.g. [29], [30], [31]).

Σ_h : Sampling covariance matrix of all (uncorrupted) latent space activations processed by the encoding function f . We use the assumption that an autoencoder can represent an inherent, sub-

dimensional structure of the data in its latent space and assume this sub-dimensional structure to sufficiently follow a multivariate Gaussian probability distribution.

Algorithm 1: Classification and Uncertainty Quantification of Corrupted Data

Input: Decoder $g : \mathbb{R}^z \rightarrow \mathbb{R}^p$; corrupted datum d ; noise covariance $\Sigma_n \in \mathbb{R}^{p \times p}$; corruption models m and C ; latent space covariance $\Sigma_h \in \mathbb{R}^{z \times z}$

Output: Classification \hat{y}_d , reconstruction uncertainty δ_r , model uncertainty δ_m ; reconstruction of uncorrupted datum $g(\bar{\mathcal{H}})$

- 1 Decouple decoder g from semi-supervised autoencoder, pretrained on uncorrupted data
 - 2 Define data model, $d = mCg(h) + n$
 - 3 Approximate $\mathcal{P}(h|d)$ with MGVI and store samples in $\mathcal{H} = \{\tilde{h}_1, \tilde{h}_2, \dots, \tilde{h}_n\}$
 - 4 Determine the sampling mean of \mathcal{H} (i.e., $\bar{\mathcal{H}}$) and classify datum directly or via M-distance to obtain \hat{y}_d
 - 5 Quantify reconstruction uncertainty with sampling standard deviation from \mathcal{H}
 - 6 Quantify model uncertainty using M-distance in the latent space
 - 7 Generate reconstruction of uncorrupted datum $g(\bar{\mathcal{H}})$
-

3 Experiments

To experimentally validate our method of classifying corrupted data with a supervised autoencoder trained on uncorrupted data, we conduct several experiments⁴ on the MNIST [32] and the Fashion-MNIST [33] dataset (both MIT-licenses, <https://opensource.org/licenses/MIT>). We evaluate the performance on various corruptions types and magnitudes and perform a comparison to MC dropout [13]. The following architecture is used for the supervised autoencoder (we use the same architecture for both datasets): A feedforward neural network is built with dimensions $784^{\{0\}} - 512^{\{1\}} - 256^{\{2\}} - 128^{\{3\}} - 10^{\{4\}} - 128^{\{5\}} - 256^{\{6\}} - 512^{\{7\}} - 784^{\{8\}}$, where layers $\{0\} - \{2\}$ and $\{4\} - \{7\}$ use the SeLU activation function [34], layer $\{3\}$ linear and layer $\{8\}$ sigmoid activations. Note that in our case, for simplicity, the number of latent space dimensions z is equal to the number of supervised classes j , although $j \leq z$ holds generally. For experiments, we train the neural network with the architecture above on two different datasets, MNIST and Fashion-MNIST. We split each dataset into three subsets, $\mathbf{X}_{\text{Train}}$ ($48 \cdot 10^3$ samples, used for training), \mathbf{X}_{Test} ($10 \cdot 10^3$ samples, used for testing and experiments) and \mathbf{X}_{Val} ($12 \cdot 10^3$ samples, used for determining Σ_h and $\Sigma_{C_k} \dots \Sigma_{C_K}$). We use Tensorflow-Keras [35] (Apache License, version 2.0, <http://www.apache.org/licenses/LICENSE-2.0>) to implement the neural networks and the MGVI implementation of NIFTy [36] (General Public License, version 3.0, <https://www.gnu.org/licenses/gpl-3.0.en.html>) to perform the inference.


3.1 Classification

We visualize experiments (1) – (3) in Figure 4. In the first experiment (1), we classify data from an independent test set of the MNIST-dataset corrupted by different noise levels with the proposed method. We compare the accuracy of our method to the baseline of processing corrupted data through the encoder of the pretrained autoencoder. We show that we significantly improve the accuracy of classifying corrupted data in comparison to the straightforward classification by $f(d)$.

For the second experiment (2), we use the same data samples as for (1) with the exception that we now additionally corrupt the data with window masking (see Appendix for visualization and details) at a constant noise level of $\alpha = 0.1$. Again, we compare the accuracy of our method to the baseline of processing the same data samples through the encoder.

In the third experiment (3), we corrupt the data by convolving them with a Gaussian blur kernel with a filter size of 7×7 and different magnitudes γ at a constant noise level of $\alpha = 0.1$.

Experiments (1), (2), and (3) lead to the following conclusions:

⁴Code to be found  [here](#).

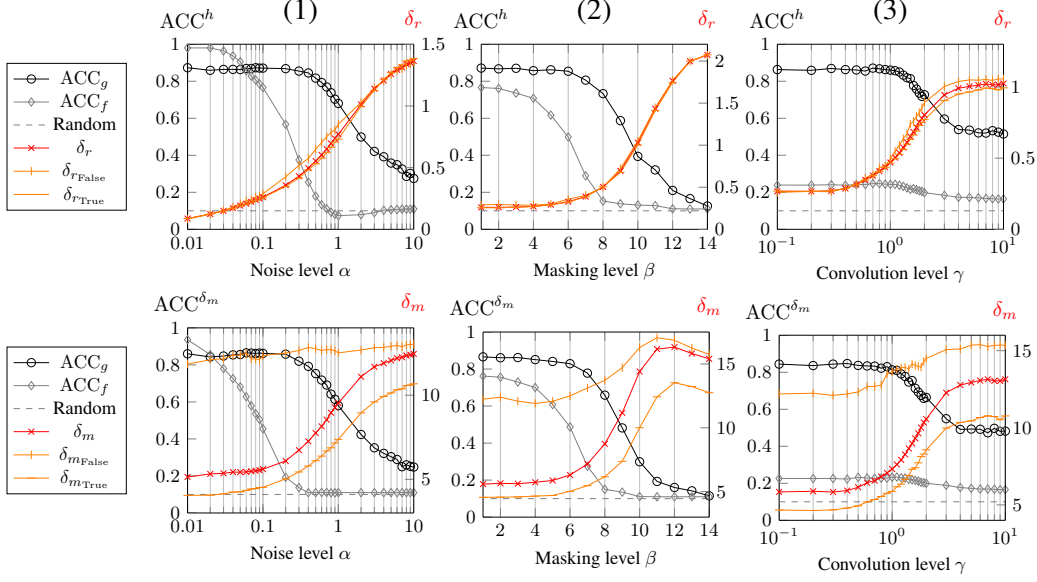


Figure 4: Accuracy and uncertainty (reconstruction uncertainty δ_r and model uncertainty δ_m) of classifications of data samples of the MNIST dataset (for Fashion-MNIST see Figure 10 in the Appendix A) at different noise levels (left column), different masking levels (middle column), and different convolution levels (right column) exploiting the supervised latent space structure (top row) and the M-distance (bottom row) as classifying features.

ACC_f serves as the baseline and is the accuracy of the plain encoding function f classifying corrupted data. ACC_g corresponds to the accuracy of the method proposed in Section 2.1. Additionally, we distinguish between uncertainties of correct classifications δ_{rTrue} , δ_{mTrue} and of false classifications δ_{rFalse} , δ_{mFalse} .

The M-distance and thus δ_m strongly depends on the quality of the classification; δ_r depends on the level of corruption and is independent of the classification result. The plot was generated with 1000 test samples for each data point (accordingly corrupted). The standard deviation is averaged over all 1000 samples.

- The reconstruction uncertainty δ_{rTrue} of correct classifications is approximately equivalent to δ_{rFalse} of wrong classifications. It is thus independent of the classification.
- Opposed to δ_r , the model uncertainty δ_m strongly depends on the correct/wrong classification of the corrupted datum: δ_m is significantly and consistently higher for false classifications than for true classifications. This delta in the model uncertainty corresponds to our method's concept of capturing the class conditional distribution density with the M-distance: For wrong classifications, the M-distance is larger because the corrupted sample is dissimilar to samples from its underlying class conditional distribution. This feature sets the basis for a statistical "lie detector" of classification and thus allows the possibility of various applications: One could pass data of high reconstruction uncertainty to further processing methods, as the process of inference is in this case likely faulty. Moreover, it is possible to pass detected false classifications with high model uncertainties to human verification. Fields of application could be the validation of neural networks in, e.g., medical imaging and other safety-critical applications.
- Classifying corrupted data through the decoder (rather than the encoder) with a suitable channel model considering the corruption significantly improves the model's accuracy without the necessity of retraining the autoencoder. Only for very low noise levels, the direct processing of the corrupted data through f performs better than our method. We observe a general loss of accuracy in the process of inference.
- Both uncertainties δ_r and δ_m rise with increasing levels of corruption, as expected. Also, the absolute value of the reconstruction uncertainty δ_r correlates inversely with the corresponding accuracy across all three experiments.

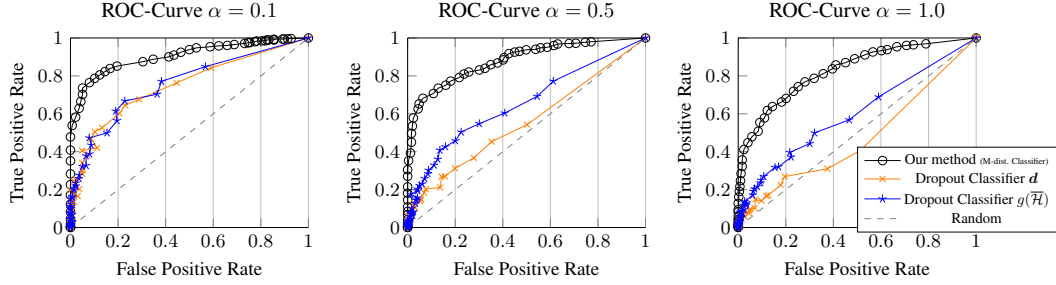


Figure 5: Receiver Operator Characteristics of the proposed identifier of false classifications for different noise levels α of our method in comparison with MC Dropout (implementation inspired by [37]) with samples from the MNIST-dataset. Left: corrupted datum at $\alpha = 0.1$. Right: corrupted datum at $\alpha = 1$. The range for ROC-Curve of Mahalanobis-Distance: $[0, 12]$. The range for ROC-Curve of overlapping samples of MC-dropout-model: $[0, 50]$. Each ROC-Curve was determined with 60 steps within the respective range, distributed uniformly. The irregularity in the ROC-Curve of the dropout model is due to the stochastic nature of MC dropout.

3.2 Detection of False Classifications

Finally, in the experiment (4) (see Figure 5), motivated by the results of experiments so far, we validate the model uncertainty of our method by evaluating the ROC-Curve of detecting false classifications with the M-distance. We detect a false classification if the minimum M-distance of a reconstructed sample in the latent space is above some threshold value. On the contrary, we detect a correct classification if the minimum M-distance is below the threshold. These threshold values vary for the plot depicted in Figure 5 between 0 and 12, being confident at 0 and uncertain at 12. We show by Figure 5 that the model uncertainty of our methodology truly reflects the confidence on a specific classification, verifying that high model uncertainty correlates with false classifications.

We compare our ROC-Curve to the ROC-Curve using the MC dropout method [13]. They exploit weight-dropout in a neural network to achieve statistically varying outputs of their classifying neural network at the same input over several forward passes. They argue that overlapping output samples indicate high uncertainty in the classification – we use the number of overlapping samples as the metric for detecting false classifications (applying 50 repetitions per sample). As [13] have not tested their model on corrupted data by noise, we pass both the decoded posterior mean for a fair comparison and the corrupted datum to the MC dropout model. The results are illustrated in Figure 5.

We make the following conclusions from experiment (4):

- Our method outperforms MC dropout to detect false classifications given the same data samples at the input. One reason for this might be that the M-distance serves as a reliable out-of-distribution detector, exploiting the inherent latent space structure of uncorrupted data as a reference, as opposed to MC-dropout. To conduct a fair experiment, we did set not only the corrupted data \mathbf{d} as the input data of MC-dropout, but also the restoration by our method, $g(\bar{\mathcal{H}})$.
- Both methods provide reliable results for detecting false classifications for low noise levels.
- The model uncertainty δ_m truly reflects the confidence of the classification, i.e., a high value of δ_m correlates empirically with a higher probability of false classification.

4 Summary and Future Research

We present a novel approach to classify heavily corrupted data with parametric classifiers trained on uncorrupted data. As we build our procedure on a probabilistic architecture, we quantify both classification and model uncertainty, allowing for a reliable detection of false classifications. We see our method as a highly flexible template that can be applied to any generative neural network to improve performance on corrupted data significantly. If the generative neural network comes with a

supervised encoded space, it can classify the data directly. We have shown that the M-distance can independently be used to classify data. Limitations of our method include that the corruption type needs to be modeled.

Future research is planned in more realistic, real-time, and complex scenarios with strong corruptions, e.g., medical imaging, autonomous driving, or astronomy. Here, potential applications of our method could be image segmentation and object detection via bounding boxes. The method described in Section 2.1 can provide uncertainties of the bounding box and thus of the position of the detected object. This might be useful, e.g., if the object of interest is occluded. A typical situation would be a car visually blocking pedestrians at a crossing.

5 Broader Impact

The methodology presented in this work deals with processing corrupted data for classification purposes and quantifying uncertainties. The approach might have an unforeseeable impact on the environments where this methodology comes to application. While the incorporation of uncertainty in parametric classifiers is generally favorable, unreliable uncertainty quantifications and classifications may lead to wrong conclusions, especially if the method claims to be certain despite a wrong classification. The chance of wrong classifications in combination with unrealistic uncertainty estimates demands an especial use of caution for all applications. Finally, the result may be influenced by unintended biases from the trained classifier and the modeled prior probability distribution.

6 Acknowledgements

The authors thank T.A. Enßlin for valuable discussions and for supporting the implementation of Bayesian inference methods. Furthermore, we thank AUDI AG and the Technical University of Munich for providing an optimal and uncomplicated research environment.

Jakob Knollmüller acknowledges the financial support by the Excellence Cluster ORIGINS, which is funded by the Deutsche Forschungsgemeinschaft (DFG, German Research Foundation) under Germany’s Excellence Strategy - EXC-2094-390783311.

References

- [1] L. Le, A. Patterson, and M. White, “Supervised Autoencoders: Improving Generalization Performance with Unsupervised Regularizers,” in *Advances in Neural Information Processing Systems*, Conference Proceedings, pp. 107–117.
- [2] J. Knom Mueller and T. Ensslin, “Metric Gaussian Variational Inference,” *arXiv pre-print server*, 2020. [Online]. Available: <https://arxiv.org/abs/1901.11033>
- [3] R. De Maesschalck, D. Jouan-Rimbaud, and D. L. Massart, “The Mahalanobis Distance,” *Chemometrics and Intelligent Laboratory Systems*, vol. 50, no. 1, pp. 1–18, 2000.
- [4] K. Lee, K. Lee, H. Lee, and J. Shin, “A Simple Unified Framework for Detecting out-of-Distribution Samples and Adversarial Attacks,” in *Advances in Neural Information Processing Systems*, Conference Proceedings, pp. 7167–7177.
- [5] V. Boehm, F. Lanusse, and U. Seljak, “Uncertainty Quantification with Generative Models,” *NeurIPS*, vol. 4th workshop on Bayesian Deep Learning, 2019. [Online]. Available: <https://arxiv.org/abs/1910.10046>
- [6] V. Böhm and U. Seljak, “Probabilistic Auto-Encoder,” *CoRR*, vol. abs/2006.05479, 2020. [Online]. Available: <https://arxiv.org/abs/2006.05479>
- [7] J. Adler and O. Öktem, “Deep Bayesian Inversion,” *CoRR*, vol. abs/1811.05910, 2018. [Online]. Available: <http://arxiv.org/abs/1811.05910>
- [8] U. Seljak and B. Yu, “Posterior Inference Unchained with EL_2O,” *CoRR*, vol. abs/1901.04454, 2019. [Online]. Available: <http://arxiv.org/abs/1901.04454>
- [9] G. Wu, J. Domke, and S. Sanner, “Conditional Inference in Pre-trained Variational Autoencoders via Cross-coding,” *CoRR*, vol. abs/1805.07785, 2018. [Online]. Available: <http://arxiv.org/abs/1805.07785>
- [10] S. Depeweg, J.-M. Hernandez-Lobato, F. Doshi-Velez, and S. Udluft, “Decomposition of Uncertainty in Bayesian deep Learning for Efficient and Risk-Sensitive Learning,” in *International Conference on Machine Learning*. PMLR, Conference Proceedings, pp. 1184–1193.
- [11] R. M. Neal, *Bayesian Learning for Neural Networks*. Springer, 1995.
- [12] T. Pearce, F. Leibfried, and A. Brintrup, “Uncertainty in Neural Networks: Approximately Bayesian Ensembling,” in *The 23rd International Conference on Artificial Intelligence and Statistics, AISTATS 2020, 26-28 August 2020, Online [Palermo, Sicily, Italy]*, ser. Proceedings of Machine Learning Research, S. Chiappa and R. Calandra, Eds., vol. 108. PMLR, 2020, pp. 234–244. [Online]. Available: <http://proceedings.mlr.press/v108/pearce20a.html>
- [13] Y. Gal and Z. Ghahramani, “Dropout as a Bayesian Approximation: Representing Model Uncertainty in Deep Learning,” p. 1050–1059, 2016.
- [14] W. Dong, L. Zhang, G. Shi, and X. Li, “Nonlocally Centralized Sparse Representation for Image Restoration,” *IEEE Transactions on Image Processing*, vol. 22, no. 4, pp. 1620–1630, 2012.
- [15] J. Lehtinen, J. Munkberg, J. Hasselgren, S. Laine, T. Karras, M. Aittala, and T. Aila, “Noise2Noise: Learning Image Restoration without Clean Data,” in *Proceedings of the 35th International Conference on Machine Learning, ICML 2018, Stockholmsmässan, Stockholm, Sweden, July 10-15, 2018*, ser. Proceedings of Machine Learning Research, J. G. Dy and A. Krause, Eds., vol. 80. PMLR, 2018, pp. 2971–2980. [Online]. Available: <http://proceedings.mlr.press/v80/lehtinen18a.html>
- [16] X. Mao, C. Shen, and Y. Yang, “Image Restoration Using Very Deep Convolutional Encoder-Decoder Networks with Symmetric Skip Connections,” in *Advances in Neural Information Processing Systems 29: Annual Conference on Neural Information Processing Systems 2016, December 5-10, 2016, Barcelona, Spain*, D. D. Lee, M. Sugiyama, U. von Luxburg, I. Guyon, and R. Garnett, Eds., 2016, pp. 2802–2810. [Online]. Available: <https://proceedings.neurips.cc/paper/2016/hash/0ed9422357395a0d4879191c66f4faa2-Abstract.html>
- [17] X. J. Mao, C. Shen, and Y. B. Yang, “Image Restoration Using Convolutional Auto-encoders with Symmetric Skip Connections,” *CoRR*, vol. abs/1606.08921, 2016. [Online]. Available: <http://arxiv.org/abs/1606.08921>

- [18] D. Zoran and Y. Weiss, "From Learning Models of Natural Image Patches to whole Image Restoration," in *2011 International Conference on Computer Vision*. IEEE, Conference Proceedings, pp. 479–486.
- [19] P. Vincent, H. Larochelle, Y. Bengio, and P.-A. Manzagol, "Extracting and composing robust features with denoising autoencoders," in *Inproceedings of the 25th International Conference on Machine learning*, Conference Proceedings, pp. 1096–1103.
- [20] D. P. Kingma and J. Ba, "Adam: A Method for Stochastic Optimization," in *3rd International Conference on Learning Representations, ICLR 2015, San Diego, CA, USA, May 7-9, 2015, Conference Track Proceedings*, Y. Bengio and Y. LeCun, Eds., 2015. [Online]. Available: <http://arxiv.org/abs/1412.6980>
- [21] D. P. Kingma and M. Welling, "Auto-Encoding Variational Bayes," in *2nd International Conference on Learning Representations, ICLR 2014, Banff, AB, Canada, April 14-16, 2014, Conference Track Proceedings*, Y. Bengio and Y. LeCun, Eds., 2014. [Online]. Available: <http://arxiv.org/abs/1312.6114>
- [22] A. Kucukelbir, D. Tran, R. Ranganath, A. Gelman, and D. M. Blei, "Automatic Differentiation Variational Inference," *The Journal of Machine Learning Research*, vol. 18, no. 1, pp. 430–474, 2017.
- [23] S. Wold, K. Esbensen, and P. Geladi, "Principal Component Analysis," *Chemometrics and Intelligent Laboratory Systems*, vol. 2, no. 1-3, pp. 37–52, 1987.
- [24] J. Herbel, T. Kacprzak, A. Amara, A. Refregier, and A. Lucchi, "Fast point spread function modeling with deep learning," *Journal of Cosmology and Astroparticle Physics*, vol. 2018, no. 07, p. 054, 2018.
- [25] H. Hu and G. de Haan, "Low Cost Robust Blur Estimator," in *2006 International Conference on Image Processing*, 2006, pp. 617–620.
- [26] J. Schlecht, K. Barnard, and B. Pryor, "Statistical Inference of Biological Structure and Point Spread Functions in 3D Microscopy," in *Third International Symposium on 3D Data Processing, Visualization, and Transmission (3DPVT'06)*, 2006, pp. 373–380.
- [27] B. Li, W. Hu, T. Wu, and S.-C. Zhu, "Modeling occlusion by discriminative and-or structures," in *Proceedings of the IEEE International Conference on Computer Vision*, 2013, pp. 2560–2567.
- [28] R. Rosales and S. Sclaroff, "Improved Tracking of Multiple Humans with Trajectory Prediction and Occlusion Modeling," Boston University Computer Science Department, Tech. Rep., 1998.
- [29] P. Gravel, G. Beaudoin, and J. A. De Guise, "A method for modeling noise in medical images," *IEEE Transactions on medical imaging*, vol. 23, no. 10, pp. 1221–1232, 2004.
- [30] X. Liu, M. Tanaka, and M. Okutomi, "Noise Level Estimation Using Weak Textured Patches of a Single Noisy Image," in *2012 19th IEEE International Conference on Image Processing*. IEEE, Conference Proceedings, pp. 665–668.
- [31] F. Russo, "A Method for Estimation and Filtering of Gaussian Noise in Images," *IEEE Transactions on Instrumentation and Measurement*, vol. 52, no. 4, pp. 1148–1154, 2003.
- [32] Y. LeCun, "The MNIST database of Handwritten Digits," <http://yann.lecun.com/exdb/mnist/>, 1998.
- [33] H. Xiao, K. Rasul, and R. Vollgraf, "Fashion-mnist: A Novel Image Dataset for Benchmarking Machine Learning Algorithms," *arXiv preprint arXiv:1708.07747*, 2017.
- [34] G. Klambauer, T. Unterthiner, A. Mayr, and S. Hochreiter, "Self-Normalizing Neural Networks," in *Advances in Neural Information Processing Systems*, Conference Proceedings, pp. 971–980.
- [35] F. Chollet *et al.*, "Keras," <https://keras.io>, 2015.
- [36] M. Selig, M. R. Bell, H. Junklewitz, N. Oppermann, M. Reinecke, M. Greiner, C. Pachajoa, and T. A. Ensslin, "NIFTY–Numerical Information Field Theory–A versatile PYTHON library for signal inference," *Astronomy & Astrophysics*, vol. 554, p. A26, 2013.
- [37] C. Park, "Code: Dropout as a Bayesian Approximation," 2019. [Online]. Available: <https://github.com/cpark321/uncertainty-deep-learning/blob/master/02.%20Dropout%20as%20a%20Bayesian%20Approximation.ipynb>
- [38] S. Depeweg, "Modeling Epistemic and Aleatoric Uncertainty with Bayesian Neural Networks and Latent Variables," Thesis, 2019.

A Appendix

A.1 Corruption Layout

Here we visualize the effect of the different corruptions, i.e., convolution as Gaussian blur C , Figure 8, masking m (Figure 7, Figure 9), and noise n , (Figure 6). We evaluate the effect of different corruption levels on accuracy and confidence, where

- α corresponds to the standard deviation of the Gaussian distribution from which noise is drawn, i.e., $\Sigma_n = \mathbf{I} \cdot \alpha$ ($\mathbf{I} \in \mathbb{R}^{p \times p}$ is the identity matrix)
- β corresponds to the number of columns and rows of pixels set to 0, counted from outside to inside (i.e., $\beta = 0$ means no masking, $\beta = 14$ means full image is masked), see figure Figure 7,
- γ corresponds to the standard deviation of the Gaussian blur kernel with a filter size of 7×7 pixels.

Note that to the experiments conducted on the effect on convolution (Figure 4, right), we added noise at $\alpha = 0.1$. For visualization purposes, we do not add noise for Figure 8.

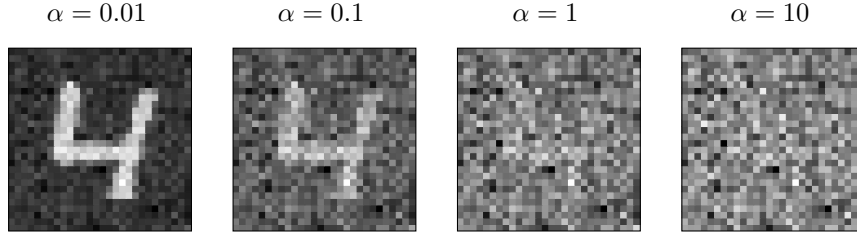


Figure 6: Exemplary visualization of corruption through noise. Experiments cover the entire noise range from $\alpha = 0.01$ to $\alpha = 10$.

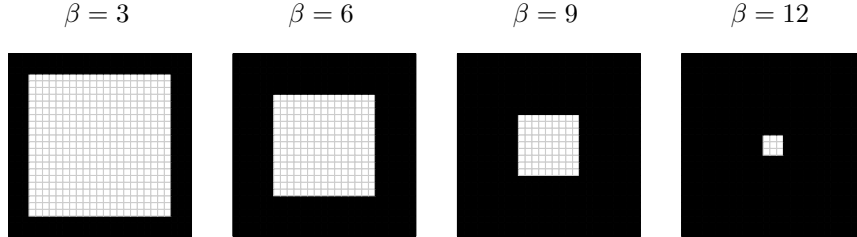


Figure 7: Exemplary visualization of isolated masking. Experiments cover the entire masking range from $\beta = 0$ to $\beta = 14$ and additional noise at $\alpha = 0.1$. The experiment layout of masking is adopted from [38].

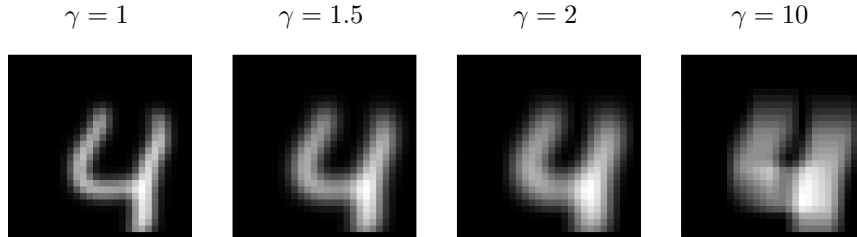


Figure 8: Exemplary visualization of corruption through convolution. Experiments cover the entire convolution range from $\gamma = 0.1$ to $\gamma = 10$.

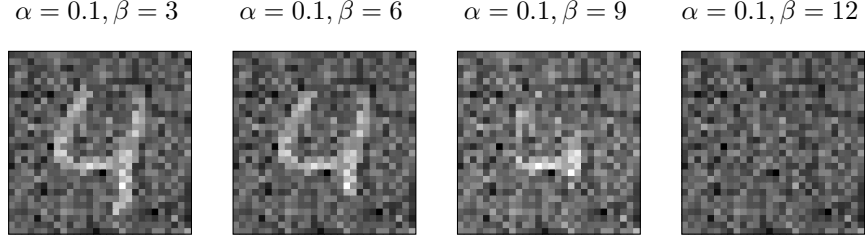


Figure 9: Exemplary visualization of different masking levels applied in experiments with additive noise $\alpha = 0.1$ on top. Experiments cover the entire masking range from $\beta = 0$ to $\beta = 14$.

A.2 Determination of the Mahalanobis-Distance

In addition to the methodology outlined in Section 2.3, we present with Algorithm 2 the pseudo-code of calculating the M-distance of the inferred latent space samples \mathcal{H} to determine the model uncertainty δ_m .

Algorithm 2: Classification and Model Uncertainty by Mahalanobis Distance

Input: Set of posterior samples $\mathcal{H} = \{\tilde{\mathbf{h}}_1, \dots, \tilde{\mathbf{h}}_n\}$; $\boldsymbol{\mu}_k, \dots, \boldsymbol{\mu}_K$; $\boldsymbol{\Sigma}_{\mathcal{C}_k}, \dots, \boldsymbol{\Sigma}_{\mathcal{C}_K}$

Output: Label of Classified Class y , model uncertainty δ_m

```

1 for  $n \leftarrow 0$  to  $N$ :
2   for  $k \leftarrow 0$  to  $K$ :
3      $\delta_m[k]_n = \sqrt{[\tilde{\mathbf{h}}_n - \boldsymbol{\mu}_k] \boldsymbol{\Sigma}_{\mathcal{C}_k}^{-1} [\tilde{\mathbf{h}}_n - \boldsymbol{\mu}_k]^T}$ 
4    $\mathcal{D}\{n\} = \delta_{m_n}$ 
5  $y = \text{argmin}(\text{mean}(\mathcal{D}))$ 
6  $\delta_m = \text{mean}(\mathcal{D})$ 
7 return  $\delta_m, y$ 

```

A.3 Experiments on Fashion-MNIST Data

Finally, we show in Figure 10 the results of the identical experiment layout of Figure 4 with Fashion-MNIST data. Note that we trained the neural network with the identical architecture as for MNIST data. Besides the general loss in the accuracy due to the retraining of the identical neural network on the more complex Fashion-MNIST dataset, the results are mostly coherent to Figure 4. In column 2, row 1, we observe that the accuracy does not further decrease for $\beta = 8$ through $\beta = 10$. We assume that this is due to the nature of the Fashion-MNIST dataset, where the window mask does not take away much information for the affected pixels: Classes such as T-shirt/top, Pullover, Dress, and Coat all usually exhibit the same structure in the affected area of the image.

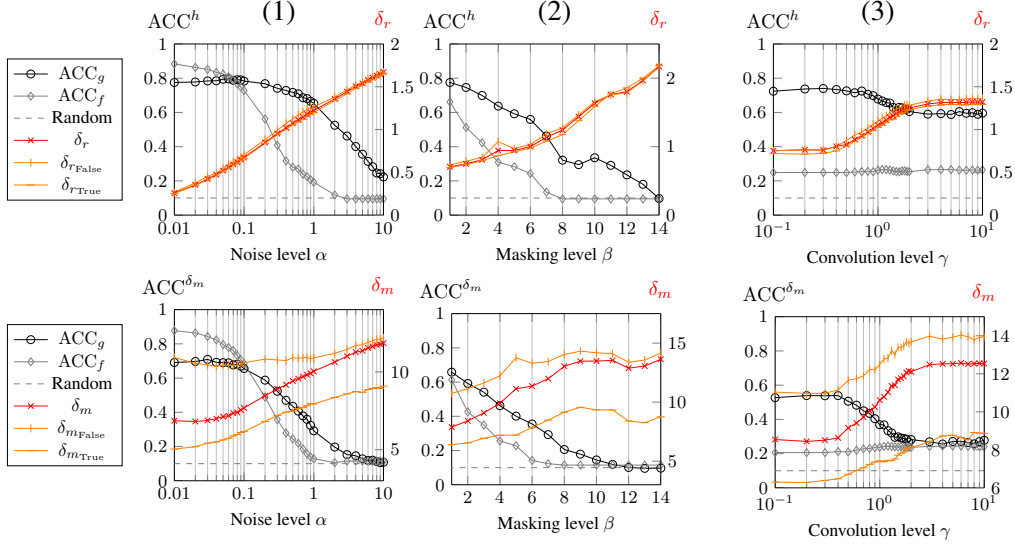


Figure 10: Accuracy and uncertainty (reconstruction uncertainty δ_r and model uncertainty δ_m) of classifications of data samples of the Fashion-MNIST dataset (for MNIST see Figure 4) at different noise levels (left column), different masking levels (middle column), and different convolution levels (right column) exploiting the supervised latent space structure (top row) and the M-distance (bottom row) as classifying features.

ACC_f serves as the baseline and is the accuracy of the plain encoding function f classifying corrupted data. ACC_g corresponds to the accuracy of the method proposed in Section 2.1. Additionally, we distinguish between uncertainties of correct classifications δ_{rTrue} , δ_{mTrue} and of false classifications δ_{rFalse} , δ_{mFalse} .